Arabian Journal of Geosciences (2022) 15: 36
https://doi.org/10.1007/s12517-021-09294-3

ORIGINAL PAPER

The effects of pore structure on the electrical properties of sand-based porous media

Weibiao Xie[1,2,3] · Qiuli Yin[3] · Xiaojiao Pang[1,2] · Guiwen Wang[1,2] · Song Wang[1,2]

Received: 1 June 2021 / Accepted: 10 December 2021 / Published online: 24 December 2021

Abstract
Electrical properties are an essential indicator of petrophysics characteristics. This study seeks to deepen the understanding of the effects of pore structure on the electrical conductivity of sand-based porous media. Taking into account the effects of pore area heterogeneity and pore geometry heterogeneity, we improve the pore equivalent model and establish a new conductivity model for sand-based porous media. Experimental data of 39 sandstone samples, partial exhibits of non-Archie phenomenon, are analyzed to verify the new conductivity model. Results show that compared with the Archie model and equivalent rock element model, the new model has higher accuracy in evaluating essential parameters, i.e., formation factor and resistivity index. In addition, analyzed by the new model, four kinds of non-Archie phenomenon found in experimental data can be attributed to four major factors: strong pore area heterogeneity, strong pore geometry heterogeneity, dispersed *n*-values, and the fluid infilling transition from tubular-like pores to micro membrane-like pores. The new model can quantitatively characterize the effects of pore structure on the electrical conductivity of sand-based porous media and has certain guidance and reference significance for the research work of petrophysics, reservoir evaluation, etc.

Keywords Pore structure · Non-Archie phenomenon · Formation factor · Resistivity index

Nomenclature

F	Formation factor, SM/SM
I	Resistivity index, SM/SM
ϕ	Total porosity, v/v
S_w	Water saturation, v/v
f_0	Pore geometry heterogeneity coefficient, dimensionless
χ_0	Pore area heterogeneity coefficient, dimensionless
p	Pore structure coefficient, dimensionless
α	Power coefficient, dimensionless
β_1	Saturation index of tubular-like pores, dimensionless
β_2	Saturation index of micro membrane-like pores, dimensionless
S_m	Area ratio of micro membrane-like pores, v/v
S_{irr}	Irreducible water saturation, v/v
σ_0	Rock conductivity with saturated-water, SM
σ_c	Conductivity of pore water, SM
Δs_0	Cross-sectional area of the pore, μm^2
Δs_1	Minimum pore area of the pore, μm^2
S_t	Area ratio of tubular-like pores, v/v
θ_1	Angle between the vertical direction of tubular-like pores section and electric field direction, rad
θ_2	Angle between the vertical direction of micro membrane-like pores section and electric field direction, rad
ϕ_e	Tubular-like porosity (ϕe=ϕSt), v/v
τ_0	Tortuosity, m/m
S_{w1}	Water saturation of tubular-like pores, v/v
S_{w2}	Water saturation of micro membrane-like pores, v/v

Responsible Editor: Domenico M. Doronzo

✉ Weibiao Xie
gareth123@126.com

✉ Guiwen Wang
wanggw@cup.edu.cn

[1] State Key Laboratory of Petroleum Resources and Prospecting, China University of Petroleum (Beijing), Beijing 102249, China

[2] College of Geosciences, China University of Petroleum (Beijing), Beijing 102249, China

[3] PetroChina Jidong Oilfield Company, Tangshan 063004, Hebei, China

a and *b*	Constant coefficients of Archie model, dimensionless
m and *n*	Cementation index and saturation index of Archie model, dimensionless
k	Pore structure efficiency of EREM model, dimensionless
k_w	Pore structure efficiency for conductive water phase of EREM model, dimensionless
S_{we}	Effective water saturation (Swe=(Sw-S_irr)/(1-S_irr)), v/v

Introduction

The electrical properties of porous media are essential characteristics in materials, rocks, geology, water resources, and other fields (Waxman and Thomas 1974; Weiss et al. 2012; Song al et. 2018). Due to an electric current can pass through a formation because it contains water with enough dissolved ions to be conductive, the conductivity of sand-based porous media depends on pore water conductivity, amount of water present, and pore structure and geometry (Schön 2011; Azizoglu et al. 2021; Chinh 2000).

Scholars have studied that when porosity decreases, pore structure can affect the electrical properties of sand-based porous media heavily (Grattoni and Dawe 1994; Mao and Gao 2000; Yue 2019,). Meanwhile, the Non-Archie phenomenon has been widely found in experimental data analysis of porous material (Verwer et al. 2011; Dunlap et al. 1991; Cai et al. 2017) . It is mainly manifested as the non-linear relationship between log$F$ and logϕ, and non-linear relationship between log$I$ and logS_w (Al-Gathe 2009; Clavier et al. 1984, Yue and Tao 2013).

To quantitatively characterize the effects of pore structure, some conductivity models have been proposed and have increased the technology of applications dramatically (Zhang et al. 2017; Hunt 2004; Xiao et al. 2013). Winsauer has reported a method for determining the tortuosity of pore channels in porous rock (Winsauer et al. 1952). Shang has established an equivalent rock element model (EREM) by a two-orthogonal components pore model (Shang et al., 2004, 2008). Hu et al. proposed a conductivity model upon trapezoidal pore (Shengfu et al. 2017). However, the pore structure is a comprehensive parameter of pore connectivity, microstructure, tortuosity, etc. (Suman and Knight 1997; Attia 2005; Man and Jing 2000). Studies to quantitatively and systematically characterize the effects of pore structure on electrical properties are rare.

This paper intends to clarify the effects of pore structure on the measured electrical response of sand-based porous media. We improve the pore equivalent model of sand-based porous media. And based on it, a new conductive model quantitatively characterizing the integrative effects of pore heterogeneity, pore geometry, and tortuosity on electrical properties is proposed. To verify the new model, experimental data of 39 rock samples, partial exhibits of non-Archie phenomena, are analyzed. Moreover, comparative analysis between the accuracy of important parameters, i.e., formation factor and resistivity index, is calculated by the new and Archie models, EREM models. Further, according to the new model, significant factors causing four kinds of non-Archie phenomenon referring to experimental data are analyzed.

The conductive model of sand-based porous material

The conductive model of sand-based porous material

In rock-based porous media, pores include micropores, small pores, and macropores. Pores are commonly equivalent to circular tubes in existing conductivity models (Herrick and Kennedy 2009; Abousrafa et al. 2009).

Figure 1 shows a SEM (scanning electron microscope) image of a complex pore structure sandstone, and pores are filled with blue glue. It can be observed that effective connecting space is composed mainly of macropores and large throats; their pore geometry can be equivalent to a tubular-like shape. However, small and micropores and micro throats are mainly thin curved sheet shapes, small film shapes, and micro-nano crack network shapes. Their pore geometry should be equivalent to a micro membrane-like shape (Xie et al. 2020).

Figure 2 shows the diagram of the improved pore equivalent model, and pore geometry is equivalent to tubular-like shape and micro membrane-like shape.

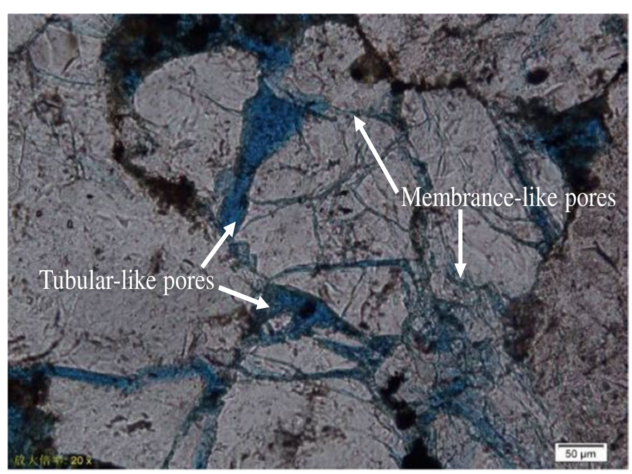

Fig. 1 Pore geometry characteristics based on SEM image

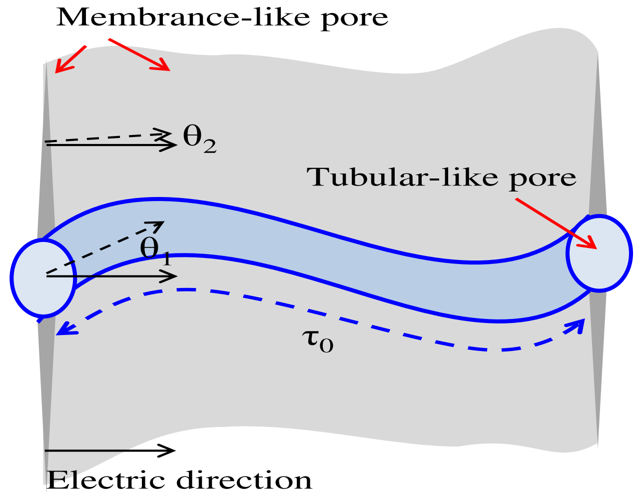

Fig. 2 Conductive diagram

In the rock per volume, the electric conductivity and total porosity are expressed as

$$\begin{cases} \sigma_0 = \dfrac{\sigma_c}{\int_0^1 \frac{1}{\Delta s_0 (S_t \cos\theta_1 + S_m \cos\theta_2)} dl} \\ \phi = \int_0^{\tau_0} \Delta s_0 dl \end{cases} \tag{1}$$

where σ_0 is the rock conductivity, ϕ is the total porosity,σ_c is the conductivity of pore water, and Δs_0 is the cross-sectional area of pore. dl is the rock section length. S_t is the area ratio of tubular-like pores. S_m is the area ratio of micro membrane-like pores. θ_1 is the angle between the vertical direction of tubular-like pores section and electric field direction. θ_2 is the angle between the vertical direction of micro membrane-like pores section and electric field direction. Generally, $\theta_1 > \theta_2$.

Introducing $p = \frac{S_m}{S_t} \frac{\cos\theta_2}{\cos\theta_1}$, the electric conductivity is obtained.

$$\sigma_0 = \frac{\sigma_c}{\int_0^1 \frac{1}{\Delta s_0 S_t \cos\theta_1 (1+p)} dl} \tag{2}$$

$$\text{As} \int_0^1 \frac{1}{\cos\theta_1} dl = \tau_0 \tag{3}$$

Equation (2) can be written as

$$\sigma_0 = \frac{\sigma_c \phi_e (1+p)}{{\tau_0}^2} \tag{4}$$

where ϕ_e is the tubular-like porosity ($\phi_e = \phi S_t$). Considering pore area heterogeneity, defining $g = \frac{\Delta s_0}{\Delta s_1}$, Δs_1 is the minimum pore area.

The electric conductivity and total porosity in Eq. (1) can be rewritten as

$$\begin{cases} \frac{\sigma_0 = \sigma_c \phi_e (1+p)}{{\tau_0}^2 \int_0^1 \frac{1}{g} dl} \\ \phi = \Delta s_1 \tau_0 \int_0^1 \frac{1}{g} dl \end{cases} \tag{5}$$

The weighted average G and harmonic average $\overline{G}$ can be obtained by integrating g and $\frac{1}{g}$ from 0 to 1.

$$\begin{cases} \frac{\int_0^1 g dl = \lim\limits_{n\to\infty} \sum_{n\to\infty}^{\infty} g(i)\Delta l = \frac{1}{n} \lim\limits_{n\to\infty} \sum_{n\to\infty}^{\infty} g(i) G}{\int_0^1 \frac{1}{g} dl = \lim\limits_{n\to\infty} \sum_{i=0}^{\infty} \frac{1}{g(i)} \Delta l = \frac{1}{n} \lim\limits_{n\to\infty} \sum_{i=0}^{\infty} \frac{1}{g(i)} 1 / \overline{G}} \end{cases} \tag{6}$$

Defining χ_0 as pore area heterogeneity coefficient. $\chi_0 = \overline{G}/G$ (generally, $\chi_0 \le 1$). When pore area heterogeneity becomes stronger, χ_0 decreases.

Defining f_0 as pore geometry heterogeneity coefficient. $f_0 = (1 + p)$ (generally, $f_0 \ge 1$). When pore geometry gets more complicated, f_0 increases.

Introducing χ_0 and f_0 into Eq. (4), the rock conductivity is rewritten as

$$\sigma_0 = \frac{\sigma_c \phi_e}{{\tau_0}^2} \chi_0 f_0 \tag{7}$$

According to Eq. (7), a conductive model quantitatively characterizing the effects of pore structure on electrical conductivity is proposed.

Formation factor F

The definition of formation factor F is the ratio of rock conductivity with saturated-water and pore water conductivity. Defining $H = \chi_0 f_0$. As tortuosity τ_0 can be expressed as a power of porosity (Rangelov and Nassiri 2018; Meng and Liu 2019). According to Eq. (7), the formation factor F can be obtained

$$F = \frac{\sigma_c}{\sigma_0} = {\phi_e}^{-\alpha} H^{-1} = {\phi_e}^{-\alpha} \left(\chi_0 f_0\right)^{-1} \tag{8}$$

where α is the power coefficient.

Resistivity index I

In water-wet rock, non-wetting fluids (oil and gas) generally have lower conductivity than pore water. When non-wetting fluid entering into pores, the distribution of pore water and conduction path changes. The pressure of tubular-like pores is generally smaller than that of membrane-like pores. When pressure increases, non-wetting fluid first enters into tubular-like pores and then enters into micro membrane-like pores.

When non-wetting fluid enters into tubular-like pores, the water saturation of tubular-like pores is expressed as

$$S_{w1} = \left(S_w - S_m\right) / \left(1 - S_m\right), (S_w \geq S_m) \tag{9}$$

With the accumulation of non-wetting fluid, equivalent conductivity tortuosity increases. The tortuosity coefficient can be expressed as

$$f = \left({S_{w1}}^{\beta_1} + p\right), (S_w \geq S_m) \tag{10}$$

where β_1 is the saturation index of tubular-like pores.

When pressure increases, non-wetting fluid enters into micro membrane-like pores, rock wettability changed, and equivalent conductivity tortuosity significantly increased. The water saturation of micro membrane-like pores and tortuosity coefficient can be expressed as

$$S_{w2} = S_w / S_m, (S_w < S_m) \tag{11}$$

$$f = {S_{w2}}^{\beta_2} p, (S_w < S_m) \tag{12}$$

where β_2 is the saturation index of micro membrane-like pores.

The resistivity index I is defined as the ratio of rock conductivity with partially water-bearing and rock conductivity with saturated water. Then bringing Eq. (8) and Eq. (10) into Eq. (7) obtains

$$\begin{cases} I = \frac{\sigma_0}{\sigma_0(S_w)} = \frac{1+p}{{S_{w1}}^{\beta_1}+p}, (S_w \geq S_m) \\ I = \frac{\sigma_0}{\sigma_0(S_w)} = \frac{1+p}{{S_{w2}}^{\beta_2} p}, (S_w < S_m) \end{cases} \tag{13}$$

where $\sigma_0(S_w)$ is the rock conductivity under saturation S_w.

Model validation

In this section, the Archie model (Eq. (15)) and EREM model (Eq. (16)) are selected for comparative analysis. Table 1 shows comparative models of electrical conductivity.

In Eq. (14), S_m is approximately equal to irreducible water saturation S_{irr} (pore water in micro membrane-like shape is mainly irreducible water). Parameter p can be calculated from experimental I when only bound water existed in rock ($S_{w1} = 0$); then, α and β_1 can be determined by the least square method with experimental data F and ϕ_e, and I and S_{w1}, respectively. Further, values of χ_0 can be calculated from experimental F.

In Eq. (15), a and b are constant coefficients, usually is 1. m is the cementation index of Archie's formula, which is usually related to the degree of sandstone cementation. n is the saturation index. m and n are usually calculated by the least square method with experimental data F and ϕ, and I, and S_w respectively.

Table 1 Comparative models of electrical conductivity

Model	Equation	Equation no	Reference
New model	$\begin{cases} F = {\phi_e}^{-\alpha}\left(\chi_0 f_0\right)^{-1} \\ I = \frac{1+p}{{S_{w1}}^{\beta_1}+p}, \left(S_w \geq S_m\right) or \frac{1+p}{{S_{w2}}^{\beta_2} p}, (S_w < S_m) \end{cases}$	(14)	This paper
Archie model	$\begin{cases} F = a\phi^{-m} \\ I = b{S_w}^{-n} \end{cases}$	(15)	G.E. Archie (1942)
EREM model	$\begin{cases} F = \frac{(1-\phi)^2}{k\phi} + \frac{1}{\phi} \\ I = \left[\frac{\left(1-S_{we}\phi\right)^2}{k_w S_{we}\phi} + \frac{1}{S_{we}\phi}\right] / \left[\frac{(1-\phi)^2}{k\phi} + \frac{1}{\phi}\right] \end{cases}$	(16)	Shang et al., 2004, 2008)

In Eq. (16), k is pore structure efficiency; k_w is pore structure efficiency for conductive water phase. k and k_w can be determined by the least square method with experimental data F and ϕ, and I and S_{we}, respectively.

Relationship between logF and logϕ

A total of 27 fine sandstone and 12 glutenite samples from Dongying formation in Huanghua Depression, China, are carried out for resistivity experiment. All of these samples are water-wetted quartz sandstone (Guo et al. 2021), and low clay content (0.01–0.06 v/v) can avoid clay's influence on resistivity. The resistivity of these 39 rock samples is measured at different water saturation states.

Figure 3 shows the log$F$-log ϕ cross plot of 27 fine sandstone samples (black points) and 12 glutenite samples (yellow points). It can be observed that when porosity is bigger than 0.15 v/v, log$F$-log ϕ relationship conforms to the Archie model, while when porosity decreases, the non-Archie phenomenon appears. At the right side of Fig. 3, sample a belongs to fine siltstone; its SEM image shows a high content of micro membrane-like pores, indicating strong pore geometry heterogeneity, while its CT (computerized tomography) section scanning face rate shows low pore area heterogeneity. Its experimental F (red star point) is below the Archie calculated F (black line). Sample b is a glutenite sample. Its SEM image shows a low content of micro membrane-like pores, while its CT section scanning face rate indicates strong pore area heterogeneity. Its experimental F (blue star point) is above the Archie calculated F (black line).

Figure 4 shows the relationship cross plot between pore area heterogeneity coefficient χ_0 and porosity. χ_0 value of fine siltstone samples (black points) ranges from 0.87 to 1.1, and the average is 0.9511. For glutenite samples (red points), χ_0 value ranges from 0.56 to 0.83, and the relationship between porosity and parameter χ_0 fitted by a least square method is $\chi_0 = 1 - 0.83855 \bullet 0.00181^{\phi}$.

Figure 5 shows a good relationship between p-value with irreducible water saturation S_{irr}. Relationships

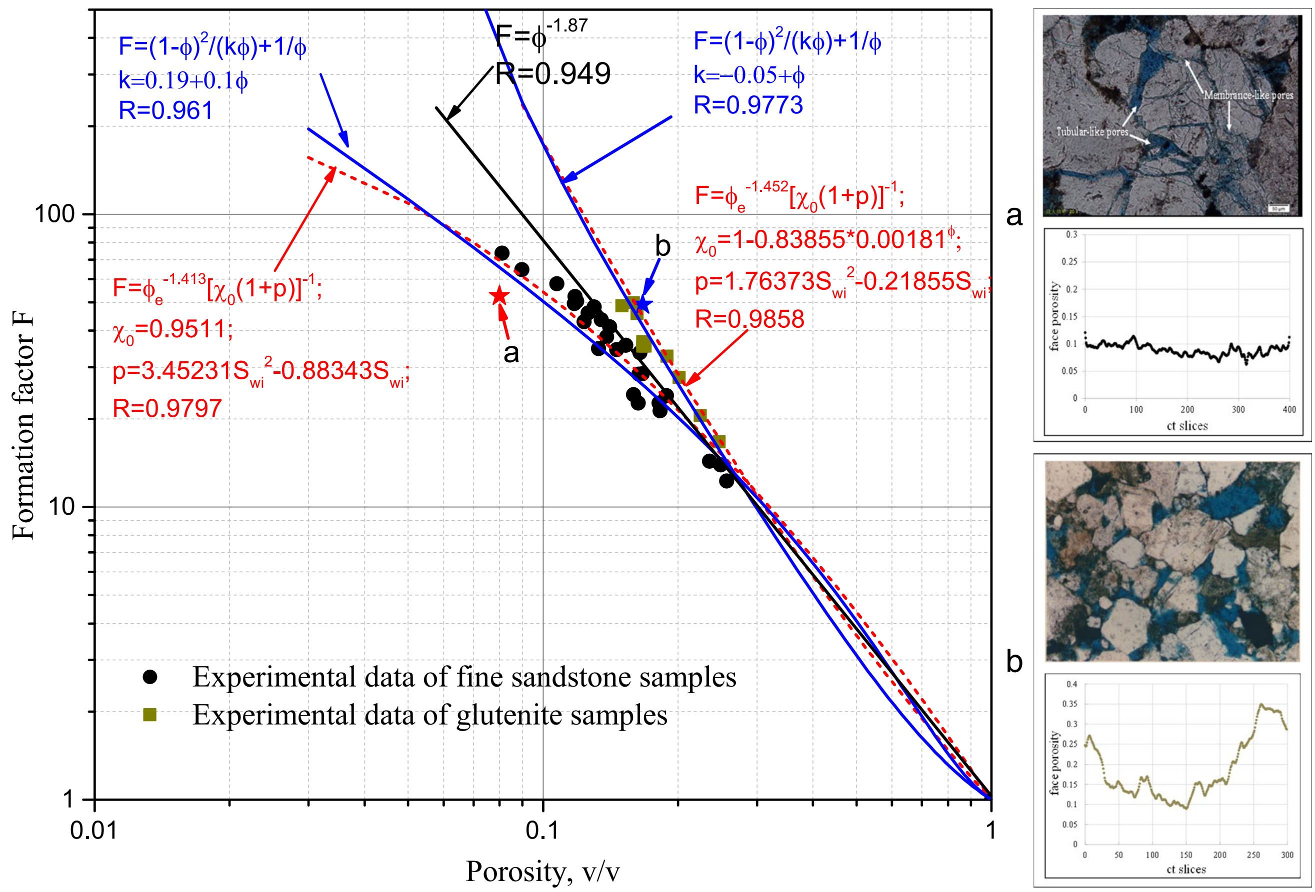

Fig. 3 **a**: SEM image and CT section scanning surface porosity rate of sample **a**. **b**: SEM image and CT section scanning surface porosity rate of sample **b**.

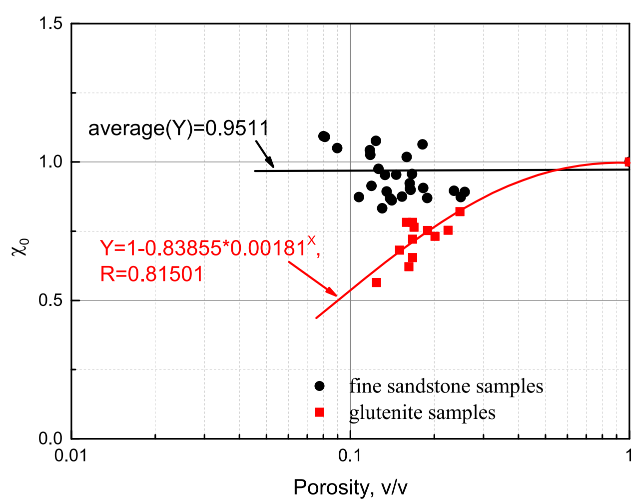

Fig. 4 Parameter χ_0 as a function of porosity

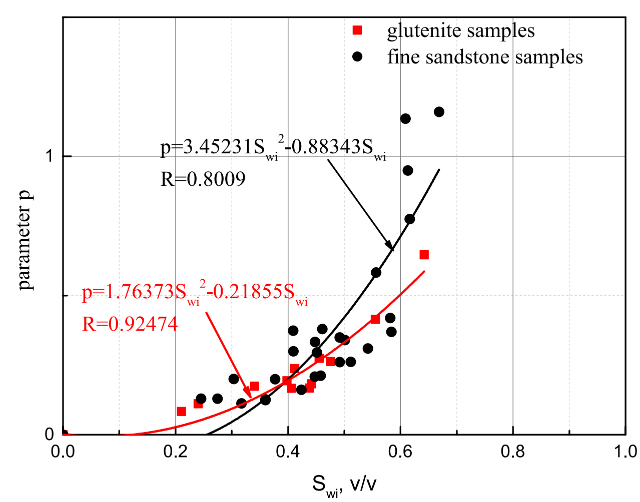

Fig. 5 Parameter p as a function of Sirr

between S_{irr} and parameter p fitted by a least square method are $p = 3.14231 \cdot S_{irr}^2 - 0.88343 S_{irr}$ in fine siltstone samples and $p = 1.76343 \cdot S_{irr}^2 - 0.21855 S_{irr}$ in glutenite samples.

Using Eqs. (14), (15), and (16) to fit the relationship between experimental formation factor and porosity of 27 fine sandstone samples respectively. Fitting result is shown in Fig. 6, and the fitting models, goodness of fit, and average

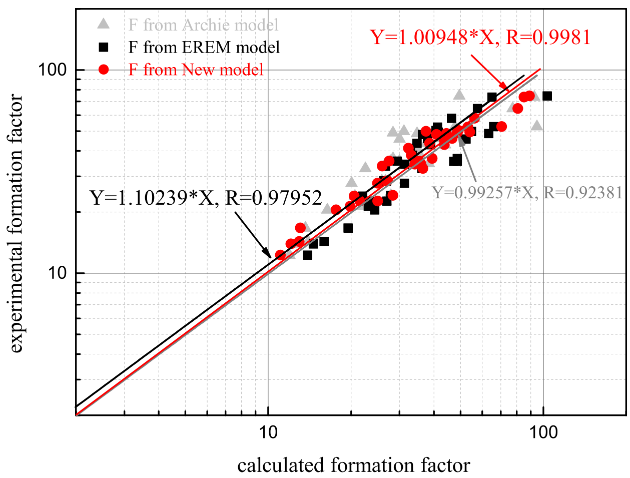

Fig. 6 Comparison between calculated *F* and experimental *F*

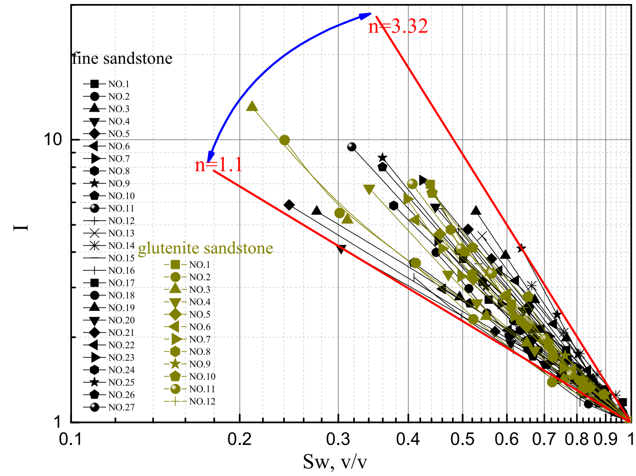

Fig. 7 Relationship between I and S_w of samples

relative error are listed in Table 2. Results show that the new model calculated formation factor is in accordance with experimental values and the accuracy is higher than that calculated by Archie and EREM models.

Relationship between logI and logS_w

Figure 7 shows the log$I$-logS_w cross plot of 39 sandstone samples (black points and yellow points in Fig. 3). Experimental *n*-values of these samples range from 1.1 to 3.32. Rapidly changing *n*-values lead to error in resistivity index I calculation by using the Archie model.

Using Eqs. (14), (15), and (16) to fit the relationship between experimental resistivity index *I* and water saturation of 27 fine sandstone samples and 12 glutenite samples, respectively. Figure 8 shows the fitting results, and Table 2 shows the fitting models, goodness of fit, average relative error, and maximum absolute error.

Figure 8 shows the comparison among the new model calculated resistivity index *I*, Archie calculated resistivity index *I*, and experimental values. Results show that the new model calculated resistivity index *I* is in accordance with experimental values and the accuracy is higher than that calculated by Archie model and EREM model.

Application

The new model (Eq. 14) is applied in Well NPX123 in Dongying Formation of Nanpu sag. NMR logging measurement mode of Well NPX123 is D9TWE3. Specific parameters are given as follows, Group A: $TW_1=12.988$ s, TEs = 0.9 ms, echo number is 500; Group B: TWs = 1 s, TEs = 0.9 ms, echo number is 500; Group C: TWc = 0.02 s, Tec = 0.6 ms, echo number is 20; Group D: $TW_1=12.988$ s, $TE_1=3.6$ ms, echo number is 125; Group E: TWs = 1 s, $TE_1=3.6$ ms, echo number is 125. Figure 9 shows the evaluation result. Drilling mud resistivity is 1.7OHMM//18 °C. $\sigma_c = 4.34\text{S/m}$, parameters are listed in Table 2.

In Fig. 9, the new model calculation results agree better with rock test results than Archie model calculation results. Compared with rock test results, the average relative error of Archie model and the new model are 6.4% and 3.2%, respectively. It can be seen that in layers 1–3, upper part of 4, which have big porosity and simple pore structure, both Archie model and new model have high calculation accuracy. While in bottom part of layer 4, layers 5–7, porosity decreased and pore structure becomes more complex, exhibiting as short range of NMR T2 spectra; calculation accuracy of the new model is significantly higher than Archie model.

Table 2 Parameters and fitting results

Model	Formation factor *F*			Resistivity index *I*		
	Equation parameters	Goodness of fit	Average relative error (%)	Equation parameters	Goodness of fit	Average relative error (%)
Archie model	$a=1, m=1.87$	0.92381	13	$b=1, n=1.713$	0.88415	11.9
EREM model	$k=0.19+0.1\varphi$ (fine sandstone) and $-0.05+\varphi$ (glutenite samples)	0.97952	10.5	$k_w = \frac{kS_{we}^{0.15}}{1+k(1-S_{we}^{0.15})}$ (fine sandstone) and $\frac{kS_{we}^{0.4}}{1+k(1-S_{we}^{0.4})}$ (glutenite samples)	0.90771	8.1
New model	$\alpha=1.413$	0.9981	10	$\beta_1=1.43$	0.98984	5.8

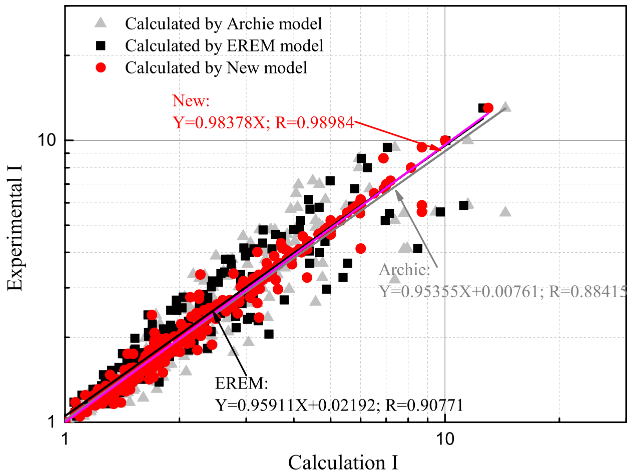

Fig. 8 Comparison between calculated I and experimental I

In Fig. 9, tracks from left to right include Tracks 1–4: natural gamma-ray logging (GR: GAPI)/spontaneous potential logging (SP: MV), depth (meters), apparent resistivity logs (RLLD/RLLS: OHMM), acoustic-wave slowness logs (AC: us/m)/bulk density (DEN: g/cm^3)/neutron porosity (CNL: %). Track 5: NMR logging T2 spectra measured with parameters TE = 0.9 ms, TW = 12,988 ms (NMR.TA: ms). Track 6: NMR logging T2 spectra measured with parameters TE = 3.6 ms, TW = 12,988 ms (NMR.TB: ms). Track 7: clay-bound water porosity computed from NMR logging (MCBW:V/V)/capillary-bound water porosity computed from NMR logging (MBVITA:V/V)/total porosity computed from NMR logging (MSIGTA: V/V)/experimental porosity of rock samples (PHIT: V/V). Track 8: permeability calculated from NMR logging (MPERM: md)/experimental permeability of rock samples (PERM: md). Track 9: irreducible water saturation computed from NMR logging (SWIRR: V/V)/experimental irreducible water saturation of rock samples (SIRR: V/V). Track 10: water saturation computed by the Archie model (SWT: V/V)/experimental oil saturation of rock samples (SO: V/V). Track 11: water saturation computed by the new model (SWX1: V/V)/experimental oil saturation of rock samples (SO: V/V). Track 12: number of the layer.

Discussion and future work

Advantages and shortages

In Eq. (8), when $H = 1$, $\alpha = m$, and S_m = 0, Eq. (14) can be simplified into the Archie model (Eq. (15)). It indicates that the new model is unified in form with the Archie model under homogeneous pure sandstone geological conditions. Parameters α and β_1 in the new model are power exponents of porosity and water saturation respectively, similar to parameters m and n in the Archie model. Compared with the conductive models simulating pores as circular tubes (Archie model) and circular-similar tubes with heterogeneous radius (EREM model), the new model takes into account the effects of pore area heterogeneity and pore geometry heterogeneity, which can more accurately reflect actual rock pore structure. As shown in Fig. 9, the new model can provide a high-precision inversion model for reservoir pore fluid volume inversion, that improves pore fluid volume calculation accuracy in sandstone reservoirs (Lai et al. 2018, 2019). After calibrating parameters α, β_1, χ_0, p in the new model by rock samples, the new model can be applied in non-sandstone reservoir evaluation, i.e., tight sandstone, carbonate rock and coal seam.

In the model validation section, the main calculation error causing factors of the new model are ① S_m is equivalent to irreducible water saturation S_{irr}; however, S_{irr} is usually larger than S_m in actual rocks. ② Measurement error of S_{irr} determined by centrifugal experiments. ③ Measurement error of rock resistivity experiments.

The main shortages of the new model are as follows: ① New model parameters χ_0 and p cannot be directly measured in rock physics experiments; they are commonly fitted by mathematic methods. ② In this paper, non-Archie phenomena is only discussed in complex pore structure quartz sandstone conditions, lacking verification and analysis of experimental data in other types of sandstone, such as feldspar sandstone and graywacke sandstone. ③ Actual pore structure is far more complicated; the new model in this paper needs to be further improved.

Non-Archie phenomenon

In this paper, the non-Archie phenomenon is manifested as non-linear. Log$F$-log ϕ relationship and non-linear. log$I$-log Sw relationship. Major factors causing the non-Archie phenomenon can be subdivided into four kinds. Analyze by the new model as follows.

a. When $H \neq 1$ and $\chi_0 < {f_0}^{-1}$ in Eq. (8), strong pore area heterogeneity causes a non-linear log$F$-log ϕ relationship and experimental formation factor is usually smaller than Archie calculated formation factor. Taking fine siltstone samples as examples, it can be seen in Fig. 5 that p-values change greatly as S_{irr} increases, indicating high content of micro membrane-like pores, while in Fig. 4, χ_0-values change little as porosity decreases, indicating low pore area heterogeneity; the experimental F (red star point) is below the Archie calculated F (black line) in Fig. 3.

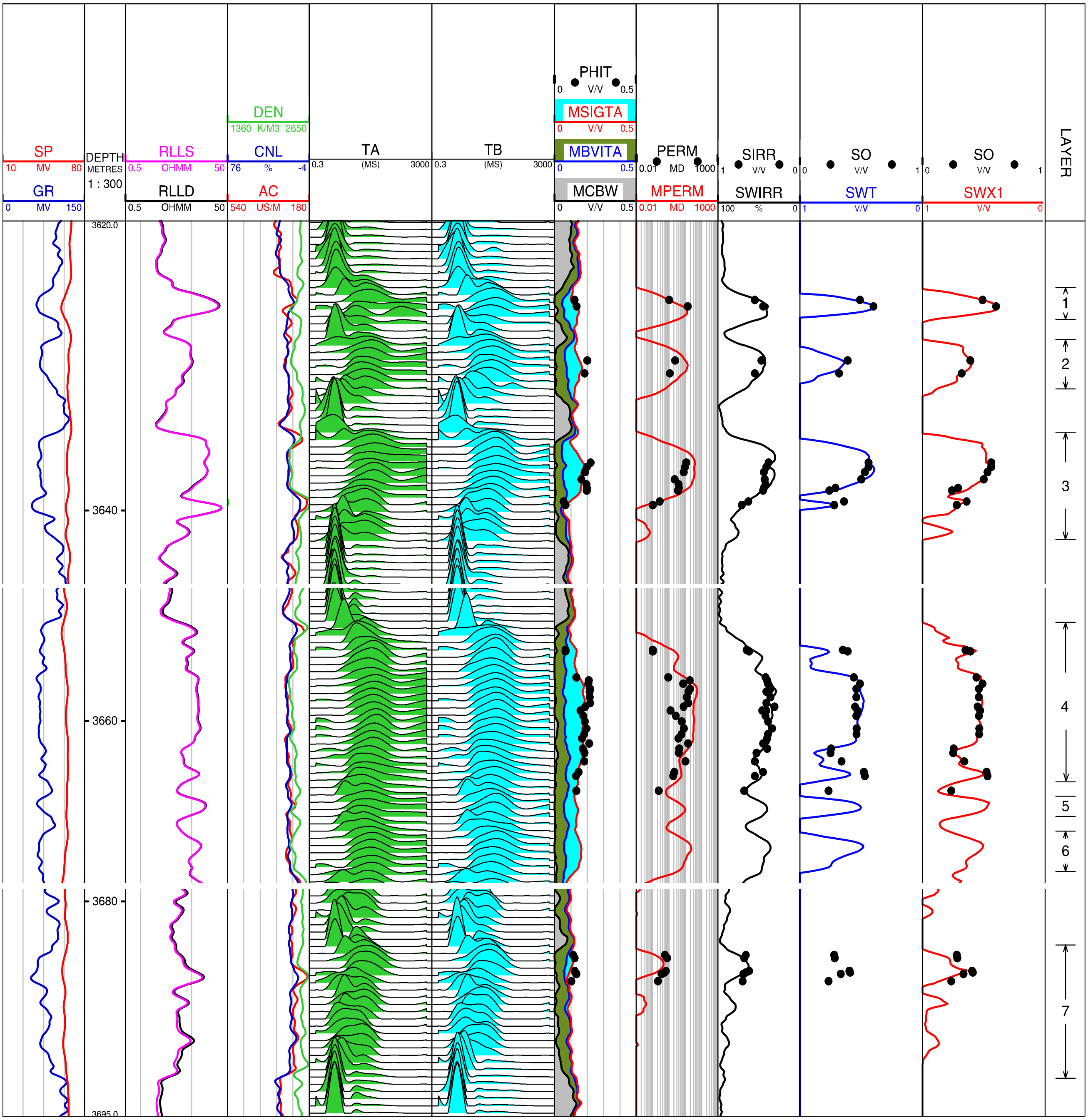

Fig. 9 Application in well NPX123 (layers 1–7)

b. When $H \neq 1$, and $\chi_0 > f_0^{-1}$ in Eq. (8), strong pore geometry heterogeneity causes a non-linear logF-log ϕ relationship and experimental formation factor is usually bigger than Archie calculated formation factor. Taking glutenite samples as examples, it can be seen in Fig. 5 that p-values change little as S_{irr} increases, indicating low content of micro membrane-like pores, while in Fig. 4, χ_0-values increase as porosity decreases, indicating strong pore area heterogeneity; the experimental F (blue star point) is above the Archie calculated F (black line) in Fig. 3.

c. As shown in Fig. 7, the dispersed n-values are manifested as the non-linear log$I$-logS_w relationship. The ratio of membrane-like pores changes greatly in different rocks; the large range of p values will lead to dispersed Archie model's n-values of different rock samples even under the same lithology conditions.

d. According to Eq. (13), when $S_w = S_m$, a corner will appear in the relationship between I and S_w. Figure 10 shows Tayor's experimental data (Taylor and Barker 2006; Worthington 2004); it can be seen that a concave exists in log$I$-logS_w relationship. Using the new model and Archie model to fit the relationship respectively, the results of new model fitting are the goodness of fit $R = 0.958$ and the average relative error 0.107. Significantly, the corner of the fitting curve existed in Fig. 10 is obvious than the experimental data. The reason may be that the actual rock pore structure is more complicated; the transition from tubular-like pores to micro membrane-like pores is a dynamic process and cannot be expressed simply as $S_w = S_m$.

Future work

Further research directions and subjects concerning electrical properties of sand-based porous material and rock conductivity model may be anticipated in:

a. Compared with sandstone, pore characteristics differ greatly in other types of rock, such as fracture and cave existed in carbonate rocks, high and low angle fracture existed in volcanic rocks, etc. (Ara et al. 2001; Gang et al. 2016). The new model needs further validation to be adaptive, and model parameters need to be determined by sample experiments.

b. The new model assumes the skeleton is not conductive; actually, some mineral skeletons in rock samples can conduct electricity, such as wet clay and pyrite (Wang and Sun 2007; Al-Sudani et al. 2020). Considering the influence of conductive minerals on rock conductivity is the next step to improving the model's accuracy.

c. Extend the application of the new model in well logging research, reservoir evaluation, reservoir research, and geological research (Mabrouk and Soliman 2015; Feng Cheng et al. 2020; Xie et al. 2021).

d. The new model can be extended and applied to cement, coal, materials, and other types of porous media (Li et al. 2016; Yurong et al. 2020; Saxena et al. 2021). Parameters of the new model need to be re-calibrated by resistivity experiments in different types of porous media.

Conclusion

In the present paper, we try to improve our understanding of how pore structure affects sand-based porous media's electrical properties. The conclusions from the study are summarized as follows:

(1) According to the pore geometry characteristics, pore geometry is equivalent to tubular-like shape and micro membrane-like shape. Based on the improved pore equivalent model, a new conductivity model of sand-based porous media is established. The new model is an extension and correction of the Archie model, and it can quantitatively characterize the effects of pore structure on electrical properties.

(2) The non-Archie phenomenon, mainly exhibiting as non-linear. Log$F$-log ϕ relationship and non-linear. log$I$-log Sw relationship is well fitted by the new model. Major reasons can be subdivided into four kinds: ① strong pore area heterogeneity causes a non-linear log$F$-log ϕ relationship and rock formation factor is usually smaller than Archie calculated formation factor.②

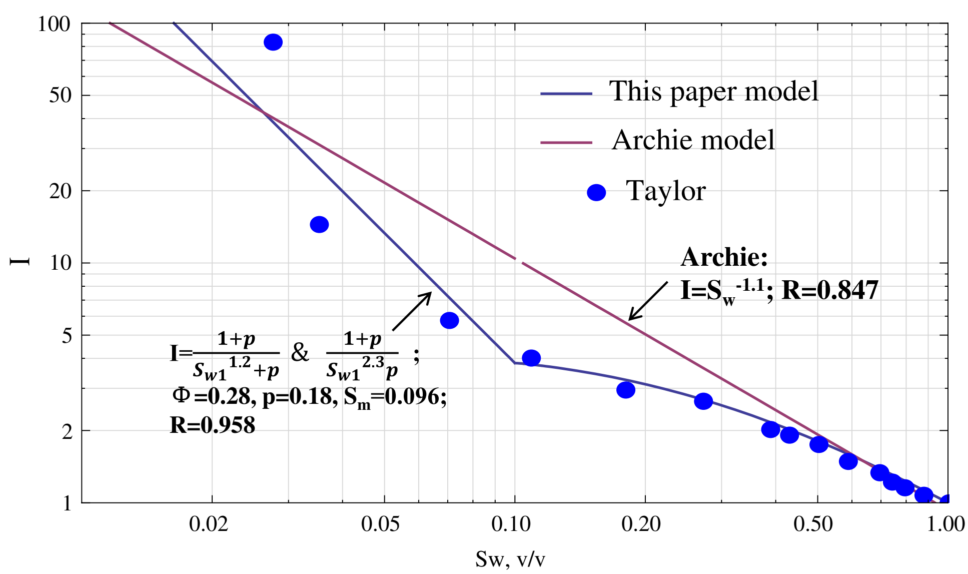

Fig. 10 Fitting results of Tayor's experimental data

Strong pore geometry heterogeneity causes a non-linear log$F$-log ϕ relationship, and rock formation factor is usually bigger than Archie calculated formation factor. ③ Dispersed n-values caused by the large range of membrane-like pore ratio cause a non-linear log$I$-log Sw relationship. ④ When non-wetting fluid enters into pores, from tubular-like pores to membrane-like pores, a corner appears in log$I$-log Sw relationship.

(3) The accuracy of the new model calculated results is higher than those calculated by the Archie and EREM models. This research has certain guidance and reference significance for petrophysics, reservoir evaluation, porous media properties, etc.

Funding This article was supported by the National Natural Science Foundation of China (No. 41872133).

Declarations

Conflict of interest The authors declare no competing interests.

References

Abousrafa EM, Somerville JM, Hamilton SA, Olden PWH, Smart BDG, Ford J (2009) Pore geometrical model for the resistivity of brine saturated rocks. J Pet Ence Eng 65(3–4):113–122

Al-Gathe A (2009) Analysis of Archie's parameters determination techniques. M.Sc Thesis. King Fahd University of Petroleum and Minerals, Saudi Arabia. 2009

Al-Sudani JA, Mustafa HK, Al-Sudani DF and Falih H (2020) Analytical water saturation model using capacitance-resistance simulation: clean and shaly formations. J Nat Gas ence Eng

Ara T, Soran T, Vaziri HH and Islam MR (2001) In-depth investigation of the validity of the archie equation in carbonate rocks. In: SPE Production and Operations Symposium, Oklahoma,(2001)24–27 March. Paper No. SPE 67204

Archie GE (1942) The electrical resistivity log as an aid in determining some reservoir characteristics. Trans AIME 146(01):54–62

Attia AM (2005) Effects of petrophysical rock properties on tortuosity factor. J Petrol Sci Eng 48(3):185–198

Azizoglu Z, Garcia AP and Heidari Z (2021) Reliable quantification of pore geometry in carbonate rocks using NMR and electrical resistivity measurements for enhanced assessment of permeability and capillary pressure. In SPWLA 62nd Annual Logging Symposium. OnePetro

Cheng Feng, Yang Zhiqiang,. et al (2020) A novel method to estimate resistivity index of tight sandstone reservoirs using nuclear magnetic resonance logs. J Nat Gas Sci Eng 79:103358

Chinh PD (2000) Electrical properties of sedimentary rocks having interconnected water-saturated pore spaces. Geophysics 65(4):1093–1097

Clavier C, Coates G, Dumanoir J (1984) Theoretical and experimental bases for the dual-water model for interpretation of shaly sands. Soc Petr Eng J 24(02):153–168

Dazhao S, Enyuan W, Qiu L, Jia H, Chen P, Wei M (2018) Response of coal rock apparent resistivity to hydraulic fracturing process. Geomech Eng 14(6):581–588

Dunlap HF, Garrouch A, Sharma MM (1991) Effects of wettability, pore geometry, and stress on electricalconduction in fluid-saturated rocks. The Log Analyst 32(05)

Gang W, Qin Y, Shen J, Hu Y, Liu D, Zhao L (2016) Resistivity response to the porosity and permeability of low rank coal. Int J Min Sci Technol 26(2):339–344

Grattoni CA, Dawe RA (1994) Pore structure influence on the electrical resistivity of saturated porous media. Proc SPE Lat Am Carib Pet Eng Conf 1994:1247–1255

Guo F, Pang X, Chen D et al (2021) Characterization of micropore structure of a middle to deep clastic reservoir: the oligocene reservoir in the Nanpu Sag, Bohai Bay Basin, China. J Pet Sci Eng 202:108567

Hunt AG (2004) Continuum percolation theory and Archie's law. Geophys Res Lett 31(19):L19503

Herrick DC, Kennedy WD (2009) A new look at electrical conduction in porous media: a physical description of rock conductivity. The SPWLA 50th Annual Logging Symposium,June 21—24,2009,paper BB

Jianchao C, Wei W, Hu X, Wood DA (2017) Electrical conductivity models in saturated porous media: a review. Earth Sci Rev 171:419–433

Jin L, Guiwen W et al (2018) Effect of pore structure on reservoir quality and oiliness in eocene dongying formation sandstones in nanpu sag, bohai bay basin, eastern china. Energy Fuels 32(9):9220–9232

Jin L, Xiaojiao P et al (2019) Origin and formation mechanisms of low oil saturation reservoirs in nanpu sag, bohai bay basin, china. Mar Pet Geol 110:317–334

Li Q, Xu S, Zeng Q (2016) The effect of water saturation degree on the electrical properties of cement-based porous material. Cement Concr Compos 70:35–47

Liang X et al (2013) Estimation of water saturation from nuclear magnetic resonance(NMR) and conventional logs in low permeability sandstone reservoirs. J Petroleum Sci Eng 108(2013):40–51

Meng H, Liu T (2019) Interpretation of the rock-electric and seepage characteristics using the pore network model. J Petrol Sci Eng 180:1–10

Man HN, Jing XD (2000) Pore network modelling of electrical resistivity and capillary pressure characteristics. Transp Porous Media 41(3):263–285

Mabrouk WM, Soliman KS (2015) A numerical technique for an accurate determination of formation resistivity factor using frrooverlays method. Arab J Geosci 8(3):1291–1297

Rangelov M, Nassiri S (2018) Empirical time-dependent tortuosity relations for hydrating mortar mixtures based on modified Archie's law. Constr Build Mater 171:825–838

Schön JH (2011) Physical Properties of Rocks: A Workbook vol. 8. The Boulevard, Langford Lane, Kidlington.Pages 198–242

Saxena N, Dietderich J, Alpak FO, Hows A, Appel M, Freeman J, ... and Zhao B (2021) Estimating electrical cementation and saturation exponents using digital rock physics. J Pet Sci Eng, 198: 108198

Suman RJ, Knight RJ (1997) Effects of pore structure and wettability on the electrical resistivity of partially saturated rocks—a network study. Geophysics 62(4):1151–1162

Shengfu Hu, Zhou C et al (2017) A tight sandstone trapezoidal pore oil saturation model. Pet Explor Dev 44(5):876–886

Shang BZ, Hamman JG, Caldwell DH (2004) A physical model to explain the first Archie Relationship and beyond. SPE Annual Technical conference and ExhIbition, Denver, Colorado. U S A.,5–8 October,2004,4

Shang BZ, Hamman JG, Caldwell DH (2008) Improved water saturation estimation using equivalent rock element model and applications to different rock types. In Europec/EAGE Conference and Exhibition. OnePetro

Taylor S, Barker R (2006) Modelling the dc electrical response of fully and partially saturated permo-triassic sandstone. Geophys Prospect 54(3):351–367

Verwer K Eberli GP Weger RJ. (2011) Effect of pore structure on electrica1 resistivity in carbonates. AAPG Bulletin 95(2):l75-190

Waxman MH, Thomas EC (1972) Electrical conductivities in Shaly Sands-I. The relation between hydrocarbon saturation and resistivity index; II. The temperature coefficient of electrical conductivity. In Fall Meeting of the Society of Petroleum Engineers of AIME. OnePetro

Weiss WJ, Snyder K, Bullard J, Bentz D (2012) Using a saturation function to interpret the electrical properties of partially saturated concrete. J Mater Civ Eng 25(8):1097–1106

Xie W, Yin Q, Guan W, Wang G, Lai J (2020) Estimating the relative permeability from the electrical parameters of sandstone with a complex pore structure. Energy Fuels 2020(34):14124–14131

Xie W, Yin Q et al (2021) Modeling and evaluation method of gas saturation based on P-wave and pore structure classification in low porosity and low permeability reservoir. Arab J Geosci 2021(14):917

Yue W (2019) Pore-scale explanation of the Archie's cementation exponent: microstructure, electrical anisotropy, and numerical experiments. Geophysical Research Letters 46(11):5799–5807

Wang KW, Sun JM, Guan JT, Zhu DW (2007) A percolation study of electrical properties of reservoir rocks. Physica A: Statistical Mechanics and its Applications 380:19–26

Winsauer WO et al (1952) Resistivity of brine-saturated sands in relation to poregeometry. AAPG Bull 36(2):253–277

Worthington PF (2004) Improved quantification of fit-for-purpose saturation exponents. SPE Reservoir Eval Eng 7(4):270–284

Yue WZ, Tao G (2013) A new non-Archie model for pore structure: numerical experiments using digital rock models. Geophys J Int 195(1):282–291

Yurong Jin, Shuxie Li, Daoyong Yang (2020) Experimental and theoretical quantification of the relationship between electrical resistivity and hydrate saturation in porous media. Fuel 269:117378

Zhang C, Cheng Y, Zhang C (2017) An improved method for predicting permeability by combining electrical measurements and mercury injection capillary pressure data. J Geophys Eng 14(1):132–142

Zhiqiang M, Chuqiang G (2000) Theoretical simulation of the resistivity and pore structure of hydrocarbon bearing rocks. Pet Explor Dev 27(2):87–90